Involvement of AMPK in regulating slow-twitch muscle atrophy during hindlimb unloading in mice

Tatsuro Egawa[1], Ayumi Goto[1,2], Yoshitaka Ohno[3], Shingo Yokoyama[3], Akihiro Ikuta[1], Miho Suzuki[1], Takao Sugiura[4], Yoshinobu Ohira[5], Toshitada Yoshioka[6], Tatsuya Hayashi[2], and Katsumasa Goto[1]

[1] Department of Physiology, Graduate School of Health Sciences, Toyohashi SOZO University, Toyohashi, Aichi, Japan

[2] Laboratory of Sports and Exercise Medicine, Graduate School of Human and Environmental Studies, Kyoto University, Kyoto, Japan

[3] Laboratory of Physiology, School of Health Sciences, Toyohashi SOZO University, Toyohashi, Aichi, Japan

[4] Department of Exercise and Sports Physiology, Faculty of Education, Yamaguchi University, Yamaguchi, Japan

[5] Graduate School of Health and Sports Science, Doshisha University, Kyotanabe, Kyoto, Japan

[6] Hirosaki Gakuin University, Hirosaki, Aomori, Japan

Short title: AMPK and unloading-induced skeletal muscle atrophy

Address for correspondence to:

Katsumasa Goto, Ph.D.

Department of Physiology, Graduate School of Health Sciences, Toyohashi SOZO

University, 20-1 Ushikawa-cho Matsushita, Toyohashi, Aichi, 440-8511, Japan

TEL: +81-50-2017-2272, FAX: +81-532-55-0803

E-mail: gotok@sepia.ocn.ne.jp

ABSTRACT

5’AMP-activated protein kinase (AMPK) is considered to have a role in regulating skeletal muscle mass. However, there are no studies investigating the function of AMPK in modulating skeletal muscle mass during atrophic conditions. In the present study, we investigated the difference in unloading-associated muscle atrophy and molecular functions in response to 2-week hindlimb suspension between transgenic mice overexpress dominant-negative mutant of AMPK (AMPK-DN) and their wild-type littermates (WT) mice. Male WT (n=24) and AMPK-DN (n=24) mice were randomly divided into two groups: untreated preexperimental control (n=12 in each group) and unloading (n=12 in each group) groups. The relative soleus muscle weight and fiber cross-sectional area to body weight were decreased by ~30% in WT mice by hindlimb unloading, while by ~20% in AMPK-DN mice. There were no changes in the indicators of protein synthesis: puromycin-labeled rotein and Akt/70-kDa ribosomal S6 kinase signaling. The expressions of ubiquitinated proteins and muscle RING finger 1 mRNA and protein, markers of ubiquitin-proteasome system, were increased by hindlimb unloading in WT mice but not in AMPK-DN mice. The expressions of molecules related to protein degradation system, phosphorylated forkhead box class O 3a, inhibitor of κBα, microRNA (miR)-1 and miR-23a were decreased in only WT mice in response to hindlimb unloading, and 72-kDa heat shock protein expression was higher in AMPK-DN mice than WT mice. These results imply that AMPK partially regulates unloading-induced atrophy of slow-twitch muscle possibly through modulating protein degradation system, especially ubiquitin-proteasome system.

Keywords: protein degradation, autophagy, ubiquitin-proteasome, microRNA, heat shock protein

INTRODUCTION

Skeletal muscle is the largest tissue in the body, accounting for approximately 40% of the total body mass, and has a crucial role in metabolism as well as locomotion. Skeletal muscle has a high ability to adapt to multiple stimuli. Increased loading such as resistance training and mechanical stretching leads to skeletal muscle hypertrophy (18, 75). In contrast, aging, poor nutrition, several diseases such as diabetes, cancer, sepsis, and chronic renal failure, and decreased loading such as inactivity, lead to skeletal muscle atrophy (23, 34, 39). Skeletal muscle atrophy occurs by the result of changes in protein turnover; decreased protein synthesis, increased protein degradation, or combination of both (17). The coordination of protein turnover in atrophic process is regulated by complicated molecular responses and the molecular mechanism involved in this process in skeletal muscle is yet completely understood and remains to be elucidated.

5'AMP-activated protein kinase (AMPK) is well established as a metabolic sensor that helps maintain cellular energy homeostasis by modulating glucose, lipid, and protein metabolism (16, 26, 28). AMPK is a heterotrimeric kinase comprising a catalytic α subunit and two regulatory subunits, β and γ. Two distinct α-isoforms (α1 and α2) are exist in mammalian cells: α1 is expressed ubiquitously, whereas α2 is dominant in skeletal muscle, heart, and liver (69). Binding of AMP to a Bateman domain of the γ-subunit of AMPK induces the allosteric activation of AMPK and phosphorylation of the Thr^{172} residue of the α-subunit, which is essential for full kinase activity (27, 59).

Several studies in the past decade suggest that AMPK has a potential role in regulating skeletal muscle mass. Gordon et al. (21, 72) provided the evidence that elevated AMPK activity was associated with diminished capacity for hypertrophy of fast-

twitch skeletal muscle in aged rat. Moreover, Paturi et al. (55) suggested that impaired hypertrophy of slow-twitch skeletal muscle during overload in diabetic rat was partly attributed to increased AMPK phosphorylation. A recent study using a knockout mouse model demonstrated that overload-induced muscle hypertrophy was accelerated in AMPKα1-deficient mice compared to the wild-type mice (50). Correspondingly, we (13) showed in vitro that stimulation with a pharmacological AMPK agonist on cultured skeletal muscle cells inhibited myotube hypertrophy and this response was attenuated in the AMPKα1/α2-knockdown condition. In addition, skeletal muscle-specific AMPKα1/α2 double knockout mice exhibit higher muscle mass than the wild-type mice in normal growth condition (37, 38). Taken together, it is suggested that AMPK is involved in the modulation of skeletal muscle mass during hypertrophic and growth conditions.

Recently, it was shown that AMPK pathway was activated in atrophic gastrocnemius muscle of mice at the early stage (3 days) of hindlimb unloading (11). However, it was not revealed whether the increase of AMPK by hindlimb unloading was directly associated with the progress of muscle atrophy. Therefore, we firstly aimed to evaluate the potential function of AMPK in skeletal muscle atrophy in response to hindlimb unloading.

AMPK is known to modify several signaling molecules that engage protein synthesis and degradation. It is accepted that AMPK inhibits mTOR signaling pathway (5), which is the major signaling pathway regulating protein synthesis. Indeed, the interaction of AMPK and mTOR signaling in regulating muscle hypertrophy was reported previously (50). On the other hand, AMPK seems to control protein degradation via two major catabolic systems in skeletal muscle; ubiquitin-proteasome (35, 52) and autophagy

systems (62) are activated by pharmacological AMPK stimulation. We (13) also demonstrated previously that AMPK inhibits hypertrophy partly through 72-kDa heat shock protein (HSP72)-mediated activation of ubiquitin-proteasome system in skeletal muscle cells. In addition, our data in the study suggested that a post-transcriptional regulation by microRNA (miRNA) might be associated with the activating process of ubiquitin-proteasome system. The discovery of miRNAs has provided a new aspect that could expand our knowledge to understand mechanisms of skeletal muscle atrophy (68, 77). Therefore, we secondly aimed to evaluate the possible involvement of these molecules in AMPK-mediated regulation of muscle mass during hindlimb unloading.

For these purpose, we examined the alterations of muscle mass and molecular responses after 2-week hindlimb unloading using transgenic mice that overexpress muscle-specific dominant-negative mutant of AMPKα1 (AMPK-DN) (44). AMPK-DN mice exhibit almost complete depletion in AMPKα2 activity and moderate depletion in AMPKα1 activity (15, 32, 44, 70). We found that loss of muscle mass in slow-twitch soleus muscle, but not fast-twitch gastrocnemius-plantaris complex and EDL muscles, of AMPK-DN mice during hindlimb unloading was less than that of wild-type littermates (WT) mice. Furthermore, we found that the adaptive responses of the molecules related to protein degradation during hindlimb unloading were attenuated in atrophic soleus muscle of AMPK-DN mice compared to WT mice. Our findings give new insights into the molecular processes involved in the skeletal muscle adaptation under atrophic conditions.

MATERIALS AND METHODS

Animals

Transgenic (AMPK-DN) mice expressing a dominant negative mutant of AMPKα1 in the skeletal muscle (44) were obtained from JCRB (Japanese Collection of Research Bioresources Cell Bank) Laboratory Animal Resource Bank at NIBIO (National Institute of Biomedical Innovation, Osaka, Japan). This strain expresses transgene introduced D157A mutation into cDNA encoding full length amino acid sequence of rat AMPK α1 subunit under the control of human α actin promoter on -2,000 bp. The heterozygous AMPK-DN mice were backcrossed with C57BL/6NCr mice, and twenty-four male AMPK-DN mice (age: 13.2 ± 3.2 weeks, body weight: 24.4 ± 1.5 g, mean ± SD) and twenty-four their WT mice (age: 13.5 ± 3.5 weeks, body weight: 23.2 ± 2.9 g, mean ± SD) were used. All mice were housed in an animal room maintained at 22-24°C with a 12:12-h light-dark cycle and fed a standard laboratory diet and water ad libitum. All animal protocols were carried out in accordance with the Guide for the Care and Use of Laboratory Animals as adopted and promulgated by the National Institutes of Health (Bethesda, MD) and were approved by the Animal Use Committee at Toyohashi SOZO University (A2012001, A2013003, A2014003). All treatments of animals were performed under anesthesia with intraperitoneal injection of sodium pentobarbital (50 mg/kg), and all efforts were made to prevent discomfort and suffering.

Procedure of hindlimb unloading

Both AMPK-DN and WT mice were randomly divided into two groups: untreated preexperimental control (n=12 in each group) and unloading (n=12 in each group) groups.

Mice of the unloading group were subjected to continuous hindlimb suspension for 2 weeks. Hindlimb suspension was performed as described previously (43). Briefly, tails of the mice were cleaned, and were loosely surrounded by adhesive tapes cross-sectionally, fixing a string on the dorsal side of the tail, to keep the blood flow intact. The string was fastened to the roof of the cage at a height allowing the forelimbs to support the weight, yet preventing the hindlimbs from touching the floor and the sides of the cage. The mice could reach food and water freely by using their forelimbs. Body weight of each mice was recorded at the end of experiment.

Protein synthesis measurements

Protein synthesis was measured by the surface sensing of translation (SUnSET) method as previously described (20). Briefly, 30 min before tissue collection, some mice (n=4 in each group) were injected intraperitoneally with puromycin (0.04 μmol/g) dissolved in 100 μl of phosphate buffered saline (PBS) under anesthesia. The expression of puromycin-labled proteins was analyzed by Western blot analyses as described below.

Tissue collection

Under anesthesia, soleus, extensor digitorum longus (EDL), and gastrocnemius-plantaris complex (GAS-PLA) muscles were dissected from each mice and weighed. We analyzed each molecule in each soleus muscle dissected from each mouse. Briefly, left soleus muscle were cross-sectionally cut into halves at the midbelly region, and proximal half of the left muscles were immediately frozen in 2-methylbutane cooled with liquid nitrogen and stored at -80°C for muscle fiber cross-sectional area (fiber CSA) analyses. Distal half of the left muscles for real-time RT-PCR analyses and right muscles for

western blot analyses and AMPK kinase assay were frozen in liquid nitrogen, and stored at -80°C.

Western blot analyses

Sample preparation and western blot analyses were performed with some modification of the previously reported method (14, 53). Briefly, the soleus muscles (>4 mg) were homogenized in 60 times its weight of ice-cold lysis buffer (CelLytic MT, Sigma-Aldrich, St. Louis, MO) with Protease/Phosphatase Inhibitor Cocktail (5872, Cell Signaling Technology, Danvers, MA) that contains inhibitors against the major classes of endogenous proteases and phosphatases. The homogenates were then sonicated and centrifuged at 16,000 g at 4°C for 15 min. The supernatants were collected for the determination of protein contents by using the Bradford technique. Protein contents in the supernatants were >420 μg in each muscle. The supernatants were solubilized in Laemmli's sample buffer containing mercaptoethanol and boiled. Samples (10 μg of protein) were separated by SDS-PAGE using a 7.5, 10, or 12% polyacrylamide gel. Proteins were then transferred to polyvinylidene difluoride membranes by using Trans-Blot Turbo transfer system (Bio-Rad Laboratories. Hercules, CA). Membranes were blocked for 1 h at room temperature in Blocking One-P (Nacalai Tesque, Kyoto, Japan) and then incubated overnight at 4°C with primary antibodies [acetyl-CoA carboxylase (ACC) Ser^{79} (3661, Cell Signaling Technology, Danvers, MA), ACC (3662, Cell Signaling Technology), Akt Ser^{473} (9271, Cell Signaling Technology), Akt (9272, Cell Signaling Technology), forkhead-box class O (FoxO) 3a Ser^{253} (9466, Cell Signaling Technology), FoxO3a (2497, Cell Signaling Technology), HSP72 (ADI-SPA-812, Enzo Life Sciences, Farmingdale, NY), heat shock transcription factor 1 (HSF1) (4356, Cell

Signaling Technology), inhibitor of κBα (IκBα) (9242, Cell Signaling Technology), microtubule-associated protein 1 light chain 3 (LC3) (2775, Cell Signaling Technology), muscle RING finger 1 (MuRF1) (GTX110475, Gene Tex, Darmstadt, Irvine, CA), puromycin (MABE343, Merck Millipore, Darmstadt, Germany), p62 (5114, Cell Signaling Technology), 70-kDa ribosomal S6 kinase (p70S6K) Thr^{389} (9234, Cell Signaling Technology), p70S6K (2708, Cell Signaling Technology), ubiquitin (3933, Cell Signaling Technology), Unc-51-like kinase 1 (Ulk1) (8054, Cell Signaling Technology), β-actin (4967, Cell Signaling Technology)] diluted in Tris buffered saline with 0.1% Tween 20 (TBS-T). The membranes were then washed with TBS-T and reacted with anti-rabbit IgG (7074, Cell Signaling Technology), or anti-mouse IgG2a (ab97245, Abcam, Cambridge, UK) for 1h at room temperature. After the final wash with TBS-T, protein bands were visualized using chemiluminescence (Wako Pure Chemical Industries, Osaka, Japan), and measured using Light-Capture (AE-6971, ATTO Corporation, Tokyo, Japan). The intensity of the signals was quantified using ImageJ software (National Institutes of Health, MD). The level of β-actin was evaluated as an internal control.

Real-time RT-PCR analyses

Real-time RT-PCR analyses were performed as was described previously (81). Briefly, total RNA was extracted from the soleus muscles (>1 mg) using the miRNeasy Mini kit (Qiagen, Hiden, Germany) according to the manufacturer's protocol. Total RNA contents in the extractions were >300 ng in each muscle. For the detection of mRNA, the RNA (200 ng) was reverse-transcribed to cDNA using PrimeScript RT Master Mix (Takara Bio), and then synthesized cDNA (4 ng) was applied to real-time RT-PCR (Thermal Cycler Dice Real Time System IIMRQ, Takara Bio) using Takara SYBR Premix

Ex Taq II (Takara Bio). For the detection of microRNA (miRNA or miR), the RNA (60 ng) was reverse-transcribed to cDNA using Mir-X^{TM} miRNA First Strand Synthesis Kit (Clontech Laboratories, Mountain View, CA), and then synthesized cDNA (4 ng) was applied to real-time RT-PCR using Mir-X^{TM} miRNA qRT-PCR SYBR Kit (Clontech Laboratories). Relative fold change of expression was calculated by the comparative CT method with Takara Thermal Cycler Dice Real Time System Software Ver. 4.00. To normalize the amount of total RNA present in each reaction, S18 ribosomal RNA (18S rRNA) for mRNA, and U6 for miRNAs were used as an internal standard.

Following primers were used: MuRF1, 5'-AGGACTCCTGCAGAGTGACCAA-3' (forward) and 5'-TTCTCGTCCAGGATGGCGTA-3' (reverse); atrogin-1/muscle atrophy F-box (MAFbx), 5'-TGTCCTTGAATTCAGCAAGCAAAC-3' (forward) and 5'-TGTGGCCATCCATTATTTCCAG-3' (reverse); 18S rRNA, 3'-ACTCAACACGGGAAACCTCA-5' (forward) and 3'-AACCAGACAAATCGCTCCAC-5' (reverse); miR-1, 5'-TGGAATGTAAAGAAGTATGTAT-3' (forward); miR-23a, 5'-ATCACATTGCCAGGGATTTCC-3' (forward); miR-133a, 5'-TTTGGTCCCCTTCAACCAGCTG-3' (forward); miR-206, 5'-TGGAATGTAAGGAAGTGTGTGG-3' (forward); miR-208b, 5'-ATAAGACGAACAAAAGGTTTGT-3' (forward); miR-499, 5'-TTAAGACTTGCAGTGATGTTT-3' (forward). The U6 primer and reverse primers for miRNA were provided with the kit.

Isoform-specific AMPK activity assay

The AMPK activity assay was performed with some modification of the previously

reported method (74). Muscles were homogenized as described in Western blot analyses, and resultant supernatants (50 μg of protein) were immunoprecipitated with isoform-specific antibodies directed against the α1 or α2 catalytic subunits of AMPK (kindly gifted by Dr. Licht Miyamoto) and protein A-Sepharose beads (GE Healthcare, Buckinghamshire, UK). Immunoprecipitates were washed twice both in wash buffer (240 mM HEPES and 480 mM NaCl). Kinase reactions were performed in the presence of synthesized and purified SAMS peptide (HMRSAMSGLHLVKRR) as AMPK substrate (74), and 40 mM HEPES (pH 7.0), 0.2 mM AMP, 80 mM NaCl, 0.8 mM dithiothreitol, 5 mM $MgCl_2$, 0.2 mM ATP (10 μCi of [γ-^{32}P] ATP/sample) (PerkinElmer, Wellesley, MA) in a final volume of 40 μl for 20 min at 30°C. At the end of the reaction, a 15-μL aliquot was removed and spotted onto Whatman P81 paper (Whatman International, Maidstone, UK). The papers were washed 6 times in 1% phosphoric acid and once in acetone. ^{32}P incorporation was quantitated with a scintillation counter, and kinase activity was expressed as fold increases relative to the basal samples.

Fiber CSA analyses

To measure the CSA of individual fibers, muscle cryostat sections were stained for laminin, a major component of the basal lamina, by the standard immunohistochemical technique (33). Briefly, serial transverse cryosections (7 μm thick) of the frozen samples were cut at –20°C and mounted on the slide glasses. Cross sections were fixed with paraformaldehyde (4%), and then were post-fixed in ice-cold methanol. After blocking by using a reagent (1% Roche Blocking Regent; Roche Diagonost, Penzberg, Germany), samples were incubated with the primary antibodies for rabbit polyclonal anti-laminin (Z0097, Dako Cytomation, Glostrup, Denmark). Sections were also incubated with the

second primary antibodies for fluorescein isothiocyanate-conjugated anti-rabbit IgG. Fiber CSA (~100 fibers/muscle) was automatically measured as the internal laminin-unstained area by using ImageJ. The relative fiber CSA to body size was normalized by body weight$^{2/3}$ according to Jaric et al. (30).

Plasma corticosterone measurement

Blood samples were collected from carotid artery into tubes containing heparin as anticoagulant, and plasma was separated by centrifugation at 8000 *g* for 15 minutes and kept at -80°C until use. Plasma level of corticosterone was measured using ELISA kit (Assaypro, St. Charles, MO).

Statistical analyses

Values were expressed as mean ± SEM. In Figure 3A, values are expressed as mean ± SD due to small numbers of animals. Statistical significance was analyzed by using two-way analysis of variance (ANOVA) with mice and treatments as main factors. If there are any significant main effects (mice and/or treatments), post-hoc multiple comparisons tests were performed between the factors (WT vs. AMPK-DN and/or untreated control vs. hindlimb unloading), and if there are any significant interactions (mice × treatments), post-hoc simple effects tests were performed among 4 groups. Post hoc analyses were conducted with Tukey-Kramer's test. Student's t-test was used to compare the percentage decrease by hindlimb unloading in muscle weight between WT and AMPK-DN (Figure 2C and 2E). The differences between groups were considered statistically significant at $P < 0.05$. The effect size (ES) was also calculated to examine whether the effect was meaningful and practically important. We interpreted the magnitude of the ES by using

conventional threshold values of 0.1 as the smallest effect, 0.3 as a moderate effect, and 0.5 as a large effect (12).

RESULTS

AMPK activity

The measurement results of AMPK activity and phosphorylation level of ACC Ser^{79}, a marker of AMPK activity, in soleus muscle are shown in Figure 1. Basal activity of AMPKα1 and AMPKα2 was lower by 20% ($p<0.05$, ES=0.66) and 95% ($p<0.05$, ES=0.97) in AMPK-DN mice than WT mice, respectively (Figure 1A). The predominant reduction of AMPKα2 activity rather than AMPKα1 activity in the transgenic mice expressing inactive α1 mutant was corresponding with the results previously reported (15, 32, 44, 70). Hindlimb unloading did not affect both AMPKα1 ($p=0.06$, ES=0.32) and AMPKα2 ($p=0.96$, ES=0.01) activity (Figure 1A). Basal expression level of phosphorylated ACC Ser^{79} was lower by 55% in AMPK-DN mice than WT mice ($p<0.05$, ES=0.73), and was not affected by hindlimb unloading ($p=0.11$, ES=0.19, Figure 1B). ACC expression was increased by hindlimb unloading ($p<0.05$, ES=0.37, Figure 1B).

Plasma corticosterone level

The changes in the plasma corticosterone level, an indicator of stress status, are shown in Table 1. The plasma corticosterone level was increased in response to hindlimb unloading ($p<0.05$, ES=0.45), but there was no difference in the levels of corticosterone between WT and AMPK-DN mice ($p=0.26$, ES=0.20, Table 1).

Body weight and muscle mass

The data of body weight and muscle mass are shown in Figure 2. The overall differences in the body weight between mice were statistically significant: the body

weight of AMPK-DN mice was slightly less compared to WT mice during experimental period ($p<0.05$, ES=0.23, Figure 2A). The body weight was reduced by hindlimb unloading ($p<0.05$, ES=0.66, Figure 2A).

Although the absolute soleus weight was reduced by hindlimb unloading ($p<0.05$, ES=0.93), the level after hindlimb unloading in AMPK-DN mice was significantly higher than in WT mice ($p<0.05$, ES=0.29, Figure 2B). The relative soleus weight to body weight was also decreased by hindlimb unloading ($p<0.05$, ES=0.77), and the level after hindlimb unloading in AMPK-DN mice was significantly higher than in WT mice ($p<0.05$, ES=0.62, Figure 2C). The degree of % changes were larger in WT mice (30%) than in AMPK-DN mice (17%) ($p<0.05$, ES=0.62, Figure 2C). Similarly, the fiber CSA of soleus muscle after hindlimb unloading was smaller than before ($p<0.05$, ES=0.89, Figure 2D). The relative fiber CSA of soleus muscle to body weight$^{2/3}$ was decreased in response to hindlimb unloading ($p<0.05$, ES=0.76), and the level after hindlimb unloading in AMPK-DN mice was significantly higher than in WT mice ($p<0.05$, ES=0.63, Figure 2E). The degree of % changes were larger in WT mice (28%) than in AMPK-DN mice (16%) ($p<0.05$, ES=0.63, Figure 2E).

The absolute EDL weight was reduced in response to hindlimb unloading ($p<0.05$, ES=0.49), and was lower in AMPK-DN mice compared to WT mice ($p<0.05$, ES=0.73, Figure 2F). The relative EDL weight to body weight was lower in AMPK-DN mice than in WT mice ($p<0.05$, ES=0.56), and no change was observed by hindlimb unloading ($p=0.07$, ES=0.27, Figure 2G). Hindlimb unloading also decreased the absolute GAS-PLA complex weight ($p<0.05$, ES=0.77) and the relative GAS-PLA complex weight to body weight ($p<0.05$, ES=0.56, Figure 2H). Both the absolute ($p<0.05$, ES=0.53) and relative ($p<0.05$, ES=0.52) GAS-PLA complex weight were lower in AMPK-DN mice

compared to WT mice (Figure 2I).

Protein synthesis pathway

Figure 3 shows the changes in the expression of puromycin-labled proteins and molecules associated with protein synthesis in soleus muscle. The expression of puromycin-labled proteins was diminished by hindlimb unloading ($p<0.05$, ES=0.61, Figure 3A). Correspondingly, the expressions of phosphorylated Akt Ser^{473} ($p<0.05$, ES=0.57, Figure 3C) and phosphorylated p70S6K Thr^{389} ($p<0.05$, ES=0.37, Figure 3D) were also decreased in response to hindlimb unloading in both mice. There were no differences in these parameters between WT and AMPK-DN mice (Akt: $p=0.77$, ES=0.04; p70S6K: $p=0.63$, ES=0.11, Figure 3C and 3D). Akt ($p<0.05$, ES=0.65, Figure 3C) but not p70S6K ($p=0.14$, ES=0.29, Figure 3D) expression was increased by hindlimb unloading.

Autophagy system

The changes in the expression of proteins related to autophagy system in soleus muscle are shown in Figure 4. Ulk1 expression was increased by hindlimb unloading in WT mice ($p<0.05$, ES=0.63), whereas it was not altered in AMPK-DN mice ($p=0.90$, ES=0.03, Figure 4B). The expression level of LC3I in AMPK-DN mice was same as that in WT mice ($p=0.41$, ES=0.15), and was not altered during hindlimb unloading ($p=0.17$, ES=0.25, Figure 4C). LC3II expression was up-regulated in WT mice ($p<0.05$, ES=0.50) by hindlimb unloading but not in AMPK-DN mice ($p=0.25$, ES=0.88, Figure 4C). The relative expression of LC3II to LC3I was increased in response to hindlimb unloading by 8.0-fold in WT mice ($p<0.05$, ES=0.58) but by 2.0-fold in AMPK-DN mice ($p=0.19$,

ES=0.50, Figure 4C). p62 expression was increased by hindlimb unloading in WT mice ($p<0.05$, ES=0.71), but not in AMPK-DN mice (p=0.59, ES=0.12, Figure 4D).

Ubiquitin-proteasome system

The variations in the expression of ubiquitinated protein and molecules related to ubiquitin-proteasome system in soleus muscle are shown in Figure 5. The accumulation of ubiquitinated proteins was observed after hindlimb unloading in WT mice ($p<0.05$, ES=0.65), but not in AMPK-DN mice (p=0.77, ES=0.07, Figure 5A). MuRF1 mRNA expression was significantly increased in response to hindlimb unloading by 4.0-fold in WT mice ($p<0.05$, ES=0.77), but not in AMPK-DN mice (p=0.28, ES=0.32, Figure 5B). The atrogin-1/MAFbx mRNA expression was up-regulated in response to hindlimb unloading ($p<0.05$, ES=0.26, Figure 5B). The protein expression of MuRF1 was also higher after hindlimb unloading in WT mice ($p<0.05$, ES=0.46), whereas there was no alteration in AMPK-DN mice (p=0.85, ES=0.06, Figure 5C).

Signaling molecules associated with protein degradation systems

The changes in the expression of proteins involved in autophagy and ubiquitin-proteasome systems in soleus muscle are shown in Figure 6. The expression of phosphorylated FoxO3a Ser^{253} was decreased by hindlimb unloading in WT mice ($p<0.05$, ES=0.65), whereas that in AMPK-DN mice was not affected by hindlimb unloading (p=0.30, ES=0.14, Figure 6B). The expression of FoxO3a was not different between the mice (p=0.46, ES=0.12) and was not changed by hindlimb unloading (p=0.17, ES=0.26, Figure 6B). The decrease of the expression level of IκBα by hindlimb unloading was observed in WT mice (p=0.07, ES=0.70), whereas there was no alteration in AMPK-DN

mice (p=0.85, ES=0.04, Figure 6C). The IκBα expression level after hindlimb unloading was higher in AMPK-DN mice than WT mice (p<0.05, ES=0.51, Figure 6C). The expression of HSP72 was constantly greater in AMPK-DN mice compared to WT mice during experiment (p<0.05, ES=0.57), and was reduced in response to hindlimb unloading by half in WT mice and by 20% in AMPK-DN mice (p<0.05, ES=0.35, Figure 6D). The expression of HSF1 was down-regulated by hindlimb unloading (p<0.05, ES=0.52, Figure 6E).

miRNA

Figure 7 shows the changes in the expression of miRNAs related to skeletal muscle atrophy in soleus muscle. The expressions of miR-1 (p<0.05, ES=0.85) and miR-23a (p<0.05, ES=0.76) were down-regulated by hindlimb unloading in WT mice while those in AMPK-DN mice were not altered (miR-1: p=0.20, ES=0.38; miR-23a: p=0.64, ES=0.13, Figure 7A and B). The expressions of miR-133a (p<0.05, ES=0.55, Figure 7C), miR-208b (p<0.05, ES=0.64, Figure 7E), and miR-499 (p<0.05, ES=0.69, Figure 7F) were reduced in response to hindlimb unloading. There was no effect by hindlimb unloading on miR-206 expression (p=0.17, ES=0.28, Figure 7D).

DISCUSSION

The present study showed that the suppression of skeletal muscle-specific AMPK activity, mainly AMPKα2 activity, partially attenuated unloading-induced atrophy of slow-twitch soleus muscle, accompanied with suppressed activation of protein degradation pathways including ubiquitin-proteasome system. To our knowledge, our findings are the first evidence that demonstrates the direct role of AMPK in skeletal muscle atrophy in vivo.

It is well known that diminished loading results in skeletal muscle atrophy (7). The hindlimb suspension rodent model was developed to mimic spaceflight-associated skeletal muscle atrophy. Furthermore, antigravitational slow soleus muscle has been used the most frequently in the experiment of unloading (22, 43, 71, 81) because it is composed more than 50% of slow-twitch fiber (78) which is more affected by reduced weight-bearing. The molecular profiling of soleus muscle in response to hindlimb suspension has significance for understanding the underlying mechanism of unloading- and disuse-associated muscle atrophy. The hindlimb suspension has also proven to be useful for investigating the physiological responses to unloading as well as disuse (47), but the suspension is some stressful procedure (48). In fact, the high corticosterone levels in plasma (Table 1) and the decrease in body weight (Figure 2A) were observed after hindlimb unloading, although the changes in plasma corticosterone and body weight in both types of mice were identical.

When the muscle weight was normalized to body weight to correct for the loss of weight after hindlimb unloading, the relative weight of soleus (Figure 2C) and GAS-PLA (Figure 2I) muscles to body weight were decreased following hindlimb unloading.

Notably, soleus muscle was atrophied by ~30% in WT mice during hindlimb unloading, while the deficiency of skeletal muscle AMPKα2 activity weakened the progress of atrophy almost by half (~17%, Figure 2C and E). In contrast, there was no difference in the degree of atrophy in GAS-PLA muscle between WT and AMPK-DN mice. These data indicate that AMPK, mainly AMPKα2, may be a crucial molecule regulating unloading-induced skeletal muscle atrophy, especially in slow-twitch muscle.

On the other hand, previous study demonstrated that AMPKα1 rather than AMPKα2 is important for regulating skeletal muscle mass in overload-induced hypertrophy (50). Although we cannot exclude the involvement of AMPKα1 in the present study; AMPKα1 activity was also lower by 20% in AMPK-DN mice (Figure 1), the different α isoforms might play a major role in regulating skeletal muscle mass under hypertrophic or atrophic stimuli.

A recent study reported that skeletal muscle AMPK signaling was up-regulated at the early stage (3 days) of hindlimb unloading and returned to basal state at 7 days in mice (11). Correspondingly, our findings showed no activation of AMPK signaling after 2-week hindlimb unloading (Figure 1). Although we did not examine the time-course changes of AMPK activity, it might be that AMPK signaling was temporary activated following hindlimb unloading and returned to basal state at 2 weeks in the present study. Moreover, it has been reported that soleus muscle atrophy during hindlimb unloading is more severe in early (~7 days) phase and moderate in latter (7~14 days) phase (3, 49). Therefore, it is speculated that the difference of the progress of soleus muscle atrophy is attributed to the suppression of AMPK activation at the early phase of hindlimb unloading.

Unloading-induced skeletal muscle atrophy is considered to be contributed partly by decreased protein synthesis (63). Akt/mammalian target of rapamycin (mTOR)/p70S6K

pathway is well established as a central regulator of protein synthesis (45), and the negative correlation of AMPK with mTOR signaling has been shown (5). Moreover, in vivo researches have demonstrated that AMPK deficiency induces overgrowth in overloaded skeletal muscle through up-regulation of mTOR signaling pathway in mice (38, 50). In the present study, however, we found that the expression of puromycin-labled proteins, an indicator of protein synthesis (20), was down-regulated in response to unloading, and this down-regulation was occurred independent of the AMPK activity (Figure 3A). Although the down-regulation was statistically significant ($p=0.001$), there was some concern that high variability of the expression in untreated control group of WT mice was observed (Figure 3A) and that this experiment was performed with small sample size ($n=4$/group). In regard to this point, we consider that this data is reliable because the effect size, a standardized index that is independent of sample size, was large ($ES=0.61$). Moreover, the phosphorylated level of Akt (activated Akt) and p70S6K (activated p70S6K) were suppressed by unloading in both mice (Figure 3B and 3C) as correspondence with the data of puromycin-labeled proteins. Taken together, it is suggested that AMPK-mediated modulation of skeletal muscle mass during unloading is controlled by another processes from protein synthesis pathway.

Interestingly, total Akt expression was increased following hindlimb unloading despite decreasing of the phosphorylated form of Akt (Figure 3C). Up-regulation of total Akt expression by 3-week hindlimb unloading in mouse muscle was previously reported (41). However, it has been shown that total Akt expression was not changed (67) or decreased (4) by 2-week hindlimb unloading in rat muscle. Total Akt alterations in response to hindlimb unloading have been controversial, and thus further investigation is required for this matter.

Increased protein degradation is contributed to unloading-induced atrophy in skeletal muscle (71). Autophagy is an important cell proteolytic system that controls protein turnover in skeletal muscle (42). The process of autophagy is regulated by multiple autophagy-related proteins. ULK1, also known as Atg1, is considered to be a key serine/threonine protein kinase acting at the early step of autophagosome formation (79). During autophagosome formation, LC3I is converted to LC3II through lipidation that allows for LC3 to become associated with autophagic vesicles. The presence of LC3 in autophagosomes and the conversion of LC3 to the lower migrating form LC3II have been used as indicators of autophagy activity (31). Recently, it has been reported that AMPK activation stimulates autophagosome formation in skeletal muscle cells (62), thus a modulation of autophagy process is possible to involve in AMPK-mediated regulation of protein degradation during unloading. In the present study, expression of Ulk1 (Figure 4B) and relative expression of LC3II to LC3I (Figure 4C) was up-regulated by unloading in WT mice, whereas the up-regulation was attenuated in the suppression of AMPK activity. These findings indicate that AMPK mediates autophagosome formation during unloading-induced skeletal muscle atrophy.

The ubiquitin-binding protein p62 which binds to LC3 is preferentially degraded by autophagy (54), and thus breakdown of p62 is generally used as a marker of autophagy flux (46). In the present study, accumulation of p62 after hindlimb unloading was also observed in WT mice but not in AMPK-DN mice (Figure 4D). This is consistent with the previous findings that p62 mRNA is up-regulated in mouse soleus (10) and gastrocnemius (11) muscle following 3-day hindlimb unloading and that p62 protein is increased by 4-week hindlimb unloading in mouse tibialis anterior and gastrocnemius muscle (40). Accumulation of p62 generally indicates an impairment of autophagy flux (46), but p62

hyperexpression was also observed in cancer cachexia-induced skeletal muscle atrophy despite the autophagy induction (56). In addition, a recent study reported the accumulation of p62 in atrophic muscle of aged mice (60). Although our findings indicate that AMPK modulates the expression of autophagy-related proteins during unloading-induced muscle atrophy, we cannot ascertain whether AMPK-mediated autophagy regulation is associated with the progress of muscle atrophy in response to hindlimb unloading.

Ubiquitin-proteasome system is also well known as a major protein degradation pathway (6). The key enzyme in this pathway is E3 ubiquitin ligases, which is responsible for protein ubiquitination. The two muscle-specific ubiquitin ligases, MuRF1 and atrogin-1/MAFbx, have been considered to be master regulators of skeletal muscle atrophy, because these genes are up-regulated in different models of muscle atrophy and have an important role in increasing protein degradation through ubiquitin-proteasome system (3, 19). Previous studies have reported that agonist-induced activation of AMPK enhances protein degradation accompanied by increased MuRF1 and atrogin-1/MAFbx mRNA expressions in cultured myotubes (35, 52). In addition, we have recently demonstrated that pharmacological activation of AMPK up-regulates MuRF1 mRNA expression and this up-regulation is abolished in AMPK-knockdown cells (13). Thus, AMPK appears to be associated with activation of ubiquitin-proteasome system, and it is possible that AMPK regulates protein degradation through ubiquitin-proteasome system during unloading. In the present study, the unloading-induced activation of ubiquitin-proteasome system, increased expressions of ubiquitinated proteins, MuRF1 mRNA and protein, was attenuated in the suppression of AMPK (Figure 5). Therefore, it is suggested that AMPK regulates ubiquitin-proteasome system-mediated protein degradation during skeletal

muscle atrophy in response to unloading.

Our findings suggest a role of AMPK that regulates unloading-induced skeletal muscle atrophy through modulating protein degradation systems. In this context, there are some possible mechanisms by which AMPK activates protein degradation systems during unloading. FoxOs are transcriptional factors that regulate transcription of genes associated with skeletal muscle homeostasis including skeletal muscle atrophy (61, 65). Previous reports have suggested that AMPK-mediated modulation of FoxO3a expression and/or nuclear translocation contributes to activation of ubiquitin-proteasome and autophagy systems in skeletal muscle cells (52, 62, 73). Thus, it is possible that AMPK regulates protein degradation systems in unloaded-associated skeletal muscle atrophy through a FoxO3a-dependent mechanism. Phosphorylation of FoxO3a at Ser^{253} results in exclusion from the nucleus and thereby inhibits the transcription activity (8). In the present study, the phosphorylation level of FoxO3a at Ser^{253} was decreased by unloading in WT mice (Figure 6B), indicating increased FoxO3a activity. This result is consistent with previous reports (25, 65). On the other hand, no change in the expression of phosphorylated FoxO3a at Ser^{253} was observed during unloading in the suppression of AMPK activity (Figure 6B), suggesting that AMPK participates in the activation of FoxO3a during skeletal muscle unloading. Therefore, FoxO3a is a possible molecule related to AMPK-mediated up-regulation of protein degradation systems in response to unloading.

On the other hand, a recent study have suggested that nuclear factor-κB (NF-κB) signaling is more important than FoxO signaling in disuse muscle atrophy (80), since NF-κB sites, but not FoxO sites, are required for the transcription of MuRF1 during hindlimb unloading. NF-κB is a transcriptional factor that is sequestered in the cytoplasm by a

family of inhibitory proteins called IκBα (51). The IκB kinase complex phosphorylates IκBα, resulting in its degradation, thereby leading to nuclear translocation of NFκB and activation. It has been reported that disruption of NFκB prevents skeletal muscle atrophy induced by hindlimb unloading (29). In the present study, the expression of IκBα tended to decrease during muscle atrophy in WT mice, and the expression was high in AMPK-DN mice compared to WT mice after hindlimb unloading (Figure 6C). These results suggest that AMPK regulates NFκB signaling via the expression of IκBα during unloading-associated muscle atrophy and this might affect the different activation of ubiquitin-proteasome system including MuRF1 expressions. To our knowledge, this is the initial report to show the association of AMPK with NFκB signaling in muscle mass regulation.

HSP72 might be another candidate molecule involved in the regulation of AMPK-mediated protein degradation systems during unloading. HSP72 is one of the most prominent member of HSPs family and considered to have an important role in preventing skeletal muscle atrophy (64). In the present study, it was observed that HSP72 expression in AMPK-DN mice was high and decreased less by unloading compared to WT mice (Figure 6D). It has been reported that overexpression of HSP72 in skeletal muscle prevents immobilization-induced atrophy in rat (66). Furthermore, a molecular mechanism of the resistance to skeletal muscle atrophy by HSP72 seems to be that HSP72 directly prevents FoxO3a activation during unloading (65, 66). We have also previously demonstrated that AMPK negatively regulates HSP72 expression in skeletal muscle cells and that HSP72 controls AMPK-mediated activation of ubiquitin-proteasome system (13). Considering these findings, it is suggested that a high expression of HSP72 due to the suppression of AMPK activity is a possible mechanism that attenuates the unloading-

induced activation of protein degradation system, partly through FoxO3a deactivation.

It has been unclear how AMPK regulates HSP72 expression. We obtained the data that HSF1, a major transcriptional factor of HSPs in mammalian skeletal muscle (82), was down-regulated following hindlimb unloading in both mice (Figure 6E), suggesting that AMPK does not modulate HSF1 expression in unloading-induced skeletal muscle atrophy. This is supported by the previous data that pharmacological activation of AMPK did not affect HSF1 expression in skeletal muscle cells (13). Thus, we consider that AMPK-mediated regulation of HSP72 during hindlimb unloading is independent of HSF1.

It has been provided evidence that a multiple miRNAs are involved in regulation of skeletal muscle atrophy (77). We have also shown that AMPK-mediated inhibition of skeletal muscle hypertrophy is accompanied by up-regulation of miR-1 (13). Therefore, we considered that miRNAs might be potent mediators of AMPK-associated regulation of muscle mass during unloading. miRNAs are short and noncoding RNA molecules approximately ~20-25 nucleotides in length that suppress gene expressions by binding to the 3'-untranslated region of target mRNAs and either inhibit translation or promote cleavage of the transcript (1, 24). Recently, it has been shown that miR-23a suppresses post-transcriptionally MuRF1 and atrogin-1/MAFbx expression in vitro and that miR-23a overexpression in mouse skeletal muscle counteracts dexamethasone-induced muscle atrophy (76). Moreover, several reports have suggested that muscle-enriched miRNAs (miR-1, miR-133a, miR-206, miR-208b, and miR-499) are associated with modulation of skeletal muscle mass. miR-1 and miR-133a are down-regulated by unloading in human skeletal muscles (57). miR-1 appears to interact with FoxO3a activity through HSP72 during dexamethasone-mediated muscle atrophy (36). miR-206 is up-regulated by denervation-induced atrophy in mice skeletal muscle, and inhibition of miR-206 partially

protects the atrophy (68). miR-208b (9) and miR-499 (2) are potential to repress the expression of myostatin, a well-known negative regulator of muscle growth (58). In the present study, miR-1 and miR-23a were down-regulated during unloading in WT mice, but these responses were not led in the suppression of AMPK activity (Figure 7). Thus, these two miRNAs, miR-1 and miR-23a, are potential to involve in the AMPK-mediated adaptation of muscle mass and its related molecules during unloading-induced atrophy. This is the first study to show the involvement of AMPK with miRNAs during atrophic condition, but knowledge about functions of the miRNAs during muscle atrophy is still limited and controversial. Our findings would help establish the function of miRNAs in regulating skeletal muscle mass.

In conclusion, we showed that the suppression of muscle-specific AMPK activity (mainly AMPKα2) partially attenuated unloading-induced atrophy of slow-twitch soleus muscle. The protective effect of muscle atrophy might be attributed to attenuation of the activity of ubiquitin-proteasome-mediated protein degradation. This is supported by the alterations of signaling molecules including FoxO3a, IκBα, HSP72, and miRNAs (miR-1 and miR-23a), although there is a limitation that these changes does not reflect dynamics of protein degradation directly. Overall, we suggest that AMPK is required for proper adaptation of muscle mass and its related molecules during skeletal muscle unloading. Further study is expected to clarify the effect of AMPK attenuation on physiological parameters such as muscle strength for a better understanding of a role of AMPK in physiological muscle functions.

ACKNOWLEDGEMENTS

We thank Liu-Lin Tang, M.D., Ph.D., Toyohashi SOZO University, for his technical assistance, and Licht Miyamoto, Ph.D., Tokushima University, for his material and technical supports. Experiment handling with radioisotopes was carried out at the Radioisotope Research Center of Kyoto University.

GRANTS

This study was supported, in part, by Grant-in-Aid for Japan Society for the Promotion of Science (JSPS) Fellows (TE and AG), Grants-in-Aid for Scientific Research from JSPS (Y Ohno, Y Ohira, TY, KG), a Research Grant from The Nakatomi Foundation (TE), The Descente Foundation for the Promotion of Sports Science (TE), and The Uehara Memorial Foundation (KG), The Naito Foundation (KG), and Graduate School of Health Sciences, Toyohashi SOZO University (KG).

DISCLOSURES

The authors state that there are no conflicts of interest.

REFERENCES

1. **Bartel DP.** MicroRNAs: genomics, biogenesis, mechanism, and function. *Cell* 116: 281-297, 2004.

2. **Bell ML, Buvoli M, and Leinwand LA.** Uncoupling of expression of an intronic microRNA and its myosin host gene by exon skipping. *Mol Cell Biol* 30: 1937-1945, 2010.

3. **Bodine SC, Latres E, Baumhueter S, Lai VK, Nunez L, Clarke BA, Poueymirou WT, Panaro FJ, Na E, Dharmarajan K, Pan ZQ, Valenzuela DM, DeChiara TM, Stitt TN, Yancopoulos GD, and Glass DJ.** Identification of ubiquitin ligases required for skeletal muscle atrophy. *Science* 294: 1704-1708, 2001.

4. **Bodine SC, Stitt TN, Gonzalez M, Kline WO, Stover GL, Bauerlein R, Zlotchenko E, Scrimgeour A, Lawrence JC, Glass DJ, and Yancopoulos GD.** Akt/mTOR pathway is a crucial regulator of skeletal muscle hypertrophy and can prevent muscle atrophy in vivo. *Nat Cell Biol* 3: 1014-1019, 2001.

5. **Bolster DR, Crozier SJ, Kimball SR, and Jefferson LS.** AMP-activated protein kinase suppresses protein synthesis in rat skeletal muscle through down-regulated mammalian target of rapamycin (mTOR) signaling. *J Biol Chem* 277: 23977-23980, 2002.

6. **Bonaldo P and Sandri M.** Cellular and molecular mechanisms of muscle atrophy. *Disease models & mechanisms* 6: 25-39, 2013.

7. **Brooks NE and Myburgh KH.** Skeletal muscle wasting with disuse atrophy is multi-dimensional: the response and interaction of myonuclei, satellite cells and signaling pathways. *Frontiers in physiology* 5: 99, 2014.

8. **Brunet A, Bonni A, Zigmond MJ, Lin MZ, Juo P, Hu LS, Anderson MJ,**

Arden KC, Blenis J, and Greenberg ME. Akt promotes cell survival by phosphorylating and inhibiting a Forkhead transcription factor. *Cell* 96: 857-868, 1999.

9. **Callis TE, Pandya K, Seok HY, Tang RH, Tatsuguchi M, Huang ZP, Chen JF, Deng Z, Gunn B, Shumate J, Willis MS, Selzman CH, and Wang DZ.** MicroRNA-208a is a regulator of cardiac hypertrophy and conduction in mice. *J Clin Invest* 119: 2772-2786, 2009.

10. **Cannavino J, Brocca L, Sandri M, Bottinelli R, and Pellegrino MA.** PGC1-alpha over-expression prevents metabolic alterations and soleus muscle atrophy in hindlimb unloaded mice. *J Physiol* 592: 4575-4589, 2014.

11. **Cannavino J, Brocca L, Sandri M, Grassi B, Bottinelli R, and Pellegrino MA.** The role of alterations in mitochondrial dynamics and PGC-1alpha over-expression in fast muscle atrophy following hindlimb unloading. *J Physiol* 593: 1981-1995, 2015.

12. **Cohen J.** *Statistical Power Analysis for the Behavioral Sciences*. Hillsdale, NJ: Lawrence Erlbaum Associates, 1988.

13. **Egawa T, Ohno Y, Goto A, Ikuta A, Suzuki M, Ohira T, Yokoyama S, Sugiura T, Ohira Y, Yoshioka T, and Goto K.** AICAR-induced activation of AMPK negatively regulates myotube hypertrophy through the HSP72-mediated pathway in C2C12 skeletal muscle cells. *Am J Physiol Endocrinol Metab* 306: E344-354, 2014.

14. **Egawa T, Tsuda S, Ma X, Hamada T, and Hayashi T.** Caffeine modulates phosphorylation of insulin receptor substrate-1 and impairs insulin signal transduction in rat skeletal muscle. *J Appl Physiol* 111: 1629-1636, 2011.

15. **Fujii N, Hirshman MF, Kane EM, Ho RC, Peter LE, Seifert MM, and Goodyear LJ.** AMP-activated protein kinase alpha2 activity is not essential for contraction- and hyperosmolarity-induced glucose transport in skeletal muscle. *J Biol*

Chem 280: 39033-39041, 2005.

16. **Fujii N, Jessen N, and Goodyear LJ.** AMP-activated protein kinase and the regulation of glucose transport. *Am J Physiol Endocrinol Metab* 291: E867-877, 2006.

17. **Goldspink DF, Garlick PJ, and McNurlan MA.** Protein turnover measured in vivo and in vitro in muscles undergoing compensatory growth and subsequent denervation atrophy. *Biochem J* 210: 89-98, 1983.

18. **Goldspink G.** Changes in muscle mass and phenotype and the expression of autocrine and systemic growth factors by muscle in response to stretch and overload. *J Anat* 194 (Pt 3): 323-334, 1999.

19. **Gomes MD, Lecker SH, Jagoe RT, Navon A, and Goldberg AL.** Atrogin-1, a muscle-specific F-box protein highly expressed during muscle atrophy. *Proc Natl Acad Sci U S A* 98: 14440-14445, 2001.

20. **Goodman CA, Mabrey DM, Frey JW, Miu MH, Schmidt EK, Pierre P, and Hornberger TA.** Novel insights into the regulation of skeletal muscle protein synthesis as revealed by a new nonradioactive in vivo technique. *FASEB J* 25: 1028-1039, 2011.

21. **Gordon SE, Lake JA, Westerkamp CM, and Thomson DM.** Does AMP-activated protein kinase negatively mediate aged fast-twitch skeletal muscle mass? *Exerc Sport Sci Rev* 36: 179-186, 2008.

22. **Goto A, Ohno Y, Ikuta A, Suzuki M, Ohira T, Egawa T, Sugiura T, Yoshioka T, Ohira Y, and Goto K.** Up-regulation of adiponectin expression in antigravitational soleus muscle in response to unloading followed by reloading, and functional overloading in mice. *PLoS One* 8: e81929, 2013.

23. **Goto K, Okuyama R, Honda M, Uchida H, Akema T, Ohira Y, and Yoshioka T.** Profiles of connectin (titin) in atrophied soleus muscle induced by unloading of rats. *J*

Appl Physiol 94: 897-902, 2003.

24. **Guller I and Russell AP.** MicroRNAs in skeletal muscle: their role and regulation in development, disease and function. *J Physiol* 588: 4075-4087, 2010.

25. **Gwag T, Lee K, Ju H, Shin H, Lee JW, and Choi I.** Stress and signaling responses of rat skeletal muscle to brief endurance exercise during hindlimb unloading: a catch-up process for atrophied muscle. *Cellular physiology and biochemistry : international journal of experimental cellular physiology, biochemistry, and pharmacology* 24: 537-546, 2009.

26. **Hardie DG.** Energy sensing by the AMP-activated protein kinase and its effects on muscle metabolism. *Proc Nutr Soc* 70: 92-99, 2011.

27. **Hawley SA, Boudeau J, Reid JL, Mustard KJ, Udd L, Makela TP, Alessi DR, and Hardie DG.** Complexes between the LKB1 tumor suppressor, STRAD alpha/beta and MO25 alpha/beta are upstream kinases in the AMP-activated protein kinase cascade. *J Biol* 2: 28, 2003.

28. **Hayashi T, Wojtaszewski JF, and Goodyear LJ.** Exercise regulation of glucose transport in skeletal muscle. *Am J Physiol* 273: E1039-1051, 1997.

29. **Hunter RB and Kandarian SC.** Disruption of either the Nfkb1 or the Bcl3 gene inhibits skeletal muscle atrophy. *J Clin Invest* 114: 1504-1511, 2004.

30. **Jaric S, Mirkov D, and Markovic G.** Normalizing physical performance tests for body size: a proposal for standardization. *Journal of strength and conditioning research / National Strength & Conditioning Association* 19: 467-474, 2005.

31. **Kabeya Y, Mizushima N, Yamamoto A, Oshitani-Okamoto S, Ohsumi Y, and Yoshimori T.** LC3, GABARAP and GATE16 localize to autophagosomal membrane depending on form-II formation. *Journal of cell science* 117: 2805-2812, 2004.

32. **Kano Y, Poole DC, Sudo M, Hirachi T, Miura S, and Ezaki O.** Control of microvascular PO(2) kinetics following onset of muscle contractions: role for AMPK. *Am J Physiol Regul Integr Comp Physiol* 301: R1350-1357, 2011.

33. **Kojima A, Goto K, Morioka S, Naito T, Akema T, Fujiya H, Sugiura T, Ohira Y, Beppu M, Aoki H, and Yoshioka T.** Heat stress facilitates the regeneration of injured skeletal muscle in rats. *Journal of orthopaedic science : official journal of the Japanese Orthopaedic Association* 12: 74-82, 2007.

34. **Kontani Y, Wang Z, Furuyama T, Sato Y, Mori N, and Yamashita H.** Effects of aging and denervation on the expression of uncoupling proteins in slow- and fast-twitch muscles of rats. *Journal of biochemistry* 132: 309-315, 2002.

35. **Krawiec BJ, Nystrom GJ, Frost RA, Jefferson LS, and Lang CH.** AMP-activated protein kinase agonists increase mRNA content of the muscle-specific ubiquitin ligases MAFbx and MuRF1 in C2C12 cells. *Am J Physiol Endocrinol Metab* 292: E1555-1567, 2007.

36. **Kukreti H, Amuthavalli K, Harikumar A, Sathiyamoorthy S, Feng PZ, Anantharaj R, Tan SL, Lokireddy S, Bonala S, Sriram S, McFarlane C, Kambadur R, and Sharma M.** Muscle-specific microRNA1 (miR1) targets heat shock protein 70 (HSP70) during dexamethasone-mediated atrophy. *J Biol Chem* 288: 6663-6678, 2013.

37. **Lantier L, Fentz J, Mounier R, Leclerc J, Treebak JT, Pehmoller C, Sanz N, Sakakibara I, Saint-Amand E, Rimbaud S, Maire P, Marette A, Ventura-Clapier R, Ferry A, Wojtaszewski JF, Foretz M, and Viollet B.** AMPK controls exercise endurance, mitochondrial oxidative capacity, and skeletal muscle integrity. *FASEB J* 28: 3211-3224, 2014.

38. **Lantier L, Mounier R, Leclerc J, Pende M, Foretz M, and Viollet B.**

Coordinated maintenance of muscle cell size control by AMP-activated protein kinase. *FASEB J* 24: 3555-3561, 2010.

39. **Lecker SH, Jagoe RT, Gilbert A, Gomes M, Baracos V, Bailey J, Price SR, Mitch WE, and Goldberg AL.** Multiple types of skeletal muscle atrophy involve a common program of changes in gene expression. *Faseb J* 18: 39-51, 2004.

40. **Liu J, Peng Y, Cui Z, Wu Z, Qian A, Shang P, Qu L, Li Y, Liu J, and Long J.** Depressed mitochondrial biogenesis and dynamic remodeling in mouse tibialis anterior and gastrocnemius induced by 4-week hindlimb unloading. *IUBMB Life* 64: 901-910, 2012.

41. **Machida M, Takeda K, Fujimaki S, Ikemune S, Nesori S, Kiyosawa H, and Takemasa T.** RNA Overshoot Accompanies Recovery of Delayed Plantaris Muscle Growth Resulting from Juvenile Hindlimb Suspension. *Advances in exercise and sports physiology* 19: 39-46, 2013.

42. **Masiero E, Agatea L, Mammucari C, Blaauw B, Loro E, Komatsu M, Metzger D, Reggiani C, Schiaffino S, and Sandri M.** Autophagy is required to maintain muscle mass. *Cell Metab* 10: 507-515, 2009.

43. **Matsuba Y, Goto K, Morioka S, Naito T, Akema T, Hashimoto N, Sugiura T, Ohira Y, Beppu M, and Yoshioka T.** Gravitational unloading inhibits the regenerative potential of atrophied soleus muscle in mice. *Acta Physiol (Oxf)* 196: 329-339, 2009.

44. **Miura S, Kai Y, Kamei Y, Bruce CR, Kubota N, Febbraio MA, Kadowaki T, and Ezaki O.** Alpha2-AMPK activity is not essential for an increase in fatty acid oxidation during low-intensity exercise. *Am J Physiol Endocrinol Metab* 296: E47-55, 2009.

45. **Miyazaki M and Esser KA.** Cellular mechanisms regulating protein synthesis

and skeletal muscle hypertrophy in animals. *J Appl Physiol* 106: 1367-1373, 2009.

46. **Mizushima N and Yoshimori T.** How to interpret LC3 immunoblotting. *Autophagy* 3: 542-545, 2007.

47. **Morey-Holton E, Globus RK, Kaplansky A, and Durnova G.** The hindlimb unloading rat model: literature overview, technique update and comparison with space flight data. *Advances in space biology and medicine* 10: 7-40, 2005.

48. **Morey-Holton ER and Globus RK.** Hindlimb unloading rodent model: technical aspects. *Journal of applied physiology* 92: 1367-1377, 2002.

49. **Morris CA, Morris LD, Kennedy AR, and Sweeney HL.** Attenuation of skeletal muscle atrophy via protease inhibition. *Journal of applied physiology* 99: 1719-1727, 2005.

50. **Mounier R, Lantier L, Leclerc J, Sotiropoulos A, Pende M, Daegelen D, Sakamoto K, Foretz M, and Viollet B.** Important role for AMPKalpha1 in limiting skeletal muscle cell hypertrophy. *FASEB J* 23: 2264-2273, 2009.

51. **Mourkioti F and Rosenthal N.** NF-kappaB signaling in skeletal muscle: prospects for intervention in muscle diseases. *Journal of molecular medicine* 86: 747-759, 2008.

52. **Nakashima K and Yakabe Y.** AMPK activation stimulates myofibrillar protein degradation and expression of atrophy-related ubiquitin ligases by increasing FOXO transcription factors in C2C12 myotubes. *Biosci Biotechnol Biochem* 71: 1650-1656, 2007.

53. **Ohno Y, Yamada S, Sugiura T, Ohira Y, Yoshioka T, and Goto K.** A possible role of NF-kappaB and HSP72 in skeletal muscle hypertrophy induced by heat stress in rats. *General physiology and biophysics* 29: 234-242, 2010.

54. **Pankiv S, Clausen TH, Lamark T, Brech A, Bruun JA, Outzen H, Overvatn A, Bjorkoy G, and Johansen T.** p62/SQSTM1 binds directly to Atg8/LC3 to facilitate degradation of ubiquitinated protein aggregates by autophagy. *J Biol Chem* 282: 24131-24145, 2007.

55. **Paturi S, Gutta AK, Kakarla SK, Katta A, Arnold EC, Wu M, Rice KM, and Blough ER.** Impaired overload-induced hypertrophy in obese Zucker rat slow-twitch skeletal muscle. *J Appl Physiol* 108: 7-13, 2010.

56. **Penna F, Costamagna D, Pin F, Camperi A, Fanzani A, Chiarpotto EM, Cavallini G, Bonelli G, Baccino FM, and Costelli P.** Autophagic degradation contributes to muscle wasting in cancer cachexia. *Am J Pathol* 182: 1367-1378, 2013.

57. **Ringholm S, Bienso RS, Kiilerich K, Guadalupe-Grau A, Aachmann-Andersen NJ, Saltin B, Plomgaard P, Lundby C, Wojtaszewski JF, Calbet JA, and Pilegaard H.** Bed rest reduces metabolic protein content and abolishes exercise-induced mRNA responses in human skeletal muscle. *Am J Physiol Endocrinol Metab* 301: E649-658, 2011.

58. **Rodriguez J, Vernus B, Chelh I, Cassar-Malek I, Gabillard JC, Hadj Sassi A, Seiliez I, Picard B, and Bonnieu A.** Myostatin and the skeletal muscle atrophy and hypertrophy signaling pathways. *Cell Mol Life Sci* 71: 4361-4371, 2014.

59. **Sakamoto K, Goransson O, Hardie DG, and Alessi DR.** Activity of LKB1 and AMPK-related kinases in skeletal muscle: effects of contraction, phenformin, and AICAR. *Am J Physiol Endocrinol Metab* 287: E310-317, 2004.

60. **Sakuma K, Kinoshita M, Ito Y, Aizawa M, Aoi W, and Yamaguchi A.** p62/SQSTM1 but not LC3 is accumulated in sarcopenic muscle of mice. *Journal of cachexia, sarcopenia and muscle*: 10.1002/jcsm.12045, 2015.

61. **Sanchez AM, Candau RB, and Bernardi H.** FoxO transcription factors: their roles in the maintenance of skeletal muscle homeostasis. *Cell Mol Life Sci* 71: 1657-1671, 2014.

62. **Sanchez AM, Csibi A, Raibon A, Cornille K, Gay S, Bernardi H, and Candau R.** AMPK promotes skeletal muscle autophagy through activation of forkhead FoxO3a and interaction with Ulk1. *J Cell Biochem* 113: 695-710, 2012.

63. **Sandri M, Sandri C, Gilbert A, Skurk C, Calabria E, Picard A, Walsh K, Schiaffino S, Lecker SH, and Goldberg AL.** Foxo transcription factors induce the atrophy-related ubiquitin ligase atrogin-1 and cause skeletal muscle atrophy. *Cell* 117: 399-412, 2004.

64. **Senf SM.** Skeletal muscle heat shock protein 70: diverse functions and therapeutic potential for wasting disorders. *Frontiers in physiology* 4: 330, 2013.

65. **Senf SM, Dodd SL, and Judge AR.** FOXO signaling is required for disuse muscle atrophy and is directly regulated by Hsp70. *Am J Physiol Cell Physiol* 298: C38-45, 2010.

66. **Senf SM, Dodd SL, McClung JM, and Judge AR.** Hsp70 overexpression inhibits NF-kappaB and Foxo3a transcriptional activities and prevents skeletal muscle atrophy. *FASEB J* 22: 3836-3845, 2008.

67. **Sitnick M, Foley AM, Brown M, and Spangenburg EE.** Ovariectomy prevents the recovery of atrophied gastrocnemius skeletal muscle mass. *Journal of applied physiology* 100: 286-293, 2006.

68. **Soares RJ, Cagnin S, Chemello F, Silvestrin M, Musaro A, De Pitta C, Lanfranchi G, and Sandri M.** Involvement of microRNAs in the regulation of muscle wasting during catabolic conditions. *J Biol Chem* 289: 21909-21925, 2014.

69. **Stapleton D, Mitchelhill KI, Gao G, Widmer J, Michell BJ, Teh T, House CM, Fernandez CS, Cox T, Witters LA, and Kemp BE.** Mammalian AMP-activated protein kinase subfamily. *J Biol Chem* 271: 611-614, 1996.

70. **Tadaishi M, Miura S, Kai Y, Kawasaki E, Koshinaka K, Kawanaka K, Nagata J, Oishi Y, and Ezaki O.** Effect of exercise intensity and AICAR on isoform-specific expressions of murine skeletal muscle PGC-1alpha mRNA: a role of beta-adrenergic receptor activation. *Am J Physiol Endocrinol Metab* 300: E341-349, 2011.

71. **Thomason DB and Booth FW.** Atrophy of the soleus muscle by hindlimb unweighting. *Journal of applied physiology* 68: 1-12, 1990.

72. **Thomson DM and Gordon SE.** Diminished overload-induced hypertrophy in aged fast-twitch skeletal muscle is associated with AMPK hyperphosphorylation. *J Appl Physiol* 98: 557-564, 2005.

73. **Tong JF, Yan X, Zhu MJ, and Du M.** AMP-activated protein kinase enhances the expression of muscle-specific ubiquitin ligases despite its activation of IGF-1/Akt signaling in C2C12 myotubes. *Journal of cellular biochemistry* 108: 458-468, 2009.

74. **Toyoda T, Hayashi T, Miyamoto L, Yonemitsu S, Nakano M, Tanaka S, Ebihara K, Masuzaki H, Hosoda K, Inoue G, Otaka A, Sato K, Fushiki T, and Nakao K.** Possible involvement of the alpha1 isoform of 5'AMP-activated protein kinase in oxidative stress-stimulated glucose transport in skeletal muscle. *Am J Physiol Endocrinol Metab* 287: E166-173, 2004.

75. **Tsika RW, Herrick RE, and Baldwin KM.** Time course adaptations in rat skeletal muscle isomyosins during compensatory growth and regression. *J Appl Physiol* 63: 2111-2121, 1987.

76. **Wada S, Kato Y, Okutsu M, Miyaki S, Suzuki K, Yan Z, Schiaffino S,**

Asahara H, Ushida T, and Akimoto T. Translational suppression of atrophic regulators by microRNA-23a integrates resistance to skeletal muscle atrophy. *J Biol Chem* 286: 38456-38465, 2011.

77. **Wang XH.** MicroRNA in myogenesis and muscle atrophy. *Curr Opin Clin Nutr Metab Care* 16: 258-266, 2013.

78. **Wigston DJ and English AW.** Fiber-type proportions in mammalian soleus muscle during postnatal development. *Journal of neurobiology* 23: 61-70, 1992.

79. **Wirth M, Joachim J, and Tooze SA.** Autophagosome formation--the role of ULK1 and Beclin1-PI3KC3 complexes in setting the stage. *Seminars in cancer biology* 23: 301-309, 2013.

80. **Wu CL, Cornwell EW, Jackman RW, and Kandarian SC.** NF-kappaB but not FoxO sites in the MuRF1 promoter are required for transcriptional activation in disuse muscle atrophy. *Am J Physiol Cell Physiol* 306: C762-767, 2014.

81. **Yasuhara K, Ohno Y, Kojima A, Uehara K, Beppu M, Sugiura T, Fujimoto M, Nakai A, Ohira Y, Yoshioka T, and Goto K.** Absence of heat shock transcription factor 1 retards the regrowth of atrophied soleus muscle in mice. *J Appl Physiol* 111: 1142-1149, 2011.

82. **Zhang Y, Huang L, Zhang J, Moskophidis D, and Mivechi NF.** Targeted disruption of hsf1 leads to lack of thermotolerance and defines tissue-specific regulation for stress-inducible Hsp molecular chaperones. *J Cell Biochem* 86: 376-393, 2002.

Tables

Table 1

Changes in the plasma corticosterone level by hindlimb unloading.

		C	HU ¶
corticosterone (ng/ml)	WT	318.7 ± 44.3	433.1 ± 64.4
	AMPK-DN	355.7 ± 33.0	504.9 ± 58.0

Values are mean ± SEM; n = 7-8 per group.

¶: post hoc multiple comparison tests following two-way ANOVA showed that the overall differences were statistically significant between untreated control (C) and hindlimb unloading (HU) groups.

WT: wild-type littermates mice, AMPK-DN: mice overexpressed muscle-specific AMPK dominant-negative

FIGURE LEGENDS

Figure 1

Changes in the 5'AMP-activated protein kinase (AMPK) activity in soleus muscle in response to hindlimb unloading. (A) isoform-specific AMPK activity. (B) phosphorylated acetyl-CoA carboxylase Ser^{79} (p-ACC) and ACC. Representative immunoblots are shown. Values are mean ± SEM. n = 8 per group. †: post hoc multiple comparisons tests following two-way ANOVA showed that the overall differences were statistically significant between wild-type littermates (WT) mice and mice overexpressed muscle-specific AMPK dominant-negative (DN), ¶: post hoc multiple comparisons tests following two-way ANOVA showed that the overall differences were statistically significant between untreated control (C) and hindlimb unloading (HU) groups.

Figure 2

Changes in the body weight, soleus weight, and muscle fiber cross-sectional area (CSA) in response to hindlimb unloading. (A) body weight (BW). (B) soleus weight. (C) relative soleus weight to BW. (D) fiber CSA in soleus. (E) relative fiber CSA to $BW^{2/3}$. (F) extensor digitorum longus (EDL) weight. (G) relative EDL weight to BW. (H) gastrocnemius-plantaris (GAS-PLA) complex weight. (I) relative GAS-PLA complex weight to BW. Representative images of immunofluorescence are shown. Scale bars indicate 20 μm. Values are mean ± SEM. n = 6-12 per group. *: post hoc simple effects tests following two-way ANOVA or Student's t test showed that the differences were statistically significant between the indicated groups. See Figure 1 for other abbreviations and symbols.

Figure 3

Changes in the protein synthesis in response to hindlimb unloading. (A) puromycin-labled protein. Values are mean ± SD. n = 4 per group. (B) representative immunoblots of phosphorylated Akt Ser^{473} (p-Akt), Akt, phosphorylated 70-kDa ribosomal S6 kinase (p70S6K) Thr^{389} (p-p70S6K) and p70S6K. (C) p-Akt and Akt. Values are mean ± SEM. n = 8 per group. (D) p-p70S6K and p70S6K. Values are mean ±SEM. n = 8 per group. See Figure 1 for abbreviations and symbols.

Figure 4

Changes in the autophagy system in response to hindlimb unloading. (A) representative immunoblots of Unc-51-like kinase 1 (Ulk1), microtubule-associated protein 1 light chain 3 (LC3) and p62. (B) Ulk1. (C) LC3. (D) p62. Values are mean ± SEM. n = 8 per group. See Figure 1 and 2 for abbreviations and symbols.

Figure 5

Changes in the ubiquitin-proteasome system in response to hindlimb unloading. (A) ubiquitinated protein. The signal intensity of full-molecular-weight ubiquitinated proteins was quantified. (B) mRNA expression of muscle RING finger 1 (MuRF1) and atrogin-1/muscle atrophy F-box (MAFbx). (C) protein expression of MuRF1. Representative immunoblots are shown. Values are mean ± SEM. n = 8 per group. See Figure 1 and 2 for abbreviations and symbols.

Figure 6

Changes in the proteins associated with protein degradation in response to hindlimb unloading. (A) representative immunoblots of phosphorylated forkhead box class O (FoxO) 3a Ser^{253} (p-FoxO3a), FoxO3a, inhibitor of κBα (IκBα), 72-kDa heat shock protein (HSP72), and heat shock transcription factor 1 (HSF1). (B) p-FoxO3a and FoxO3a. (C) IκBα. (D) HSP72. (E) HSF1. Values are mean ± SEM. n = 8 per group. See Figure 1 and 2 for abbreviations and symbols.

Figure 7

Changes in the microRNA (miR) expressions in response to hindlimb unloading. (A) miR-1. (B) miR-23a. (C) miR-133a. (D) miR-206. (E) miR-208b. (F) miR-499. Values are mean ± SEM. n = 8 per group. See Figure 1 and 2 for abbreviations and symbols.

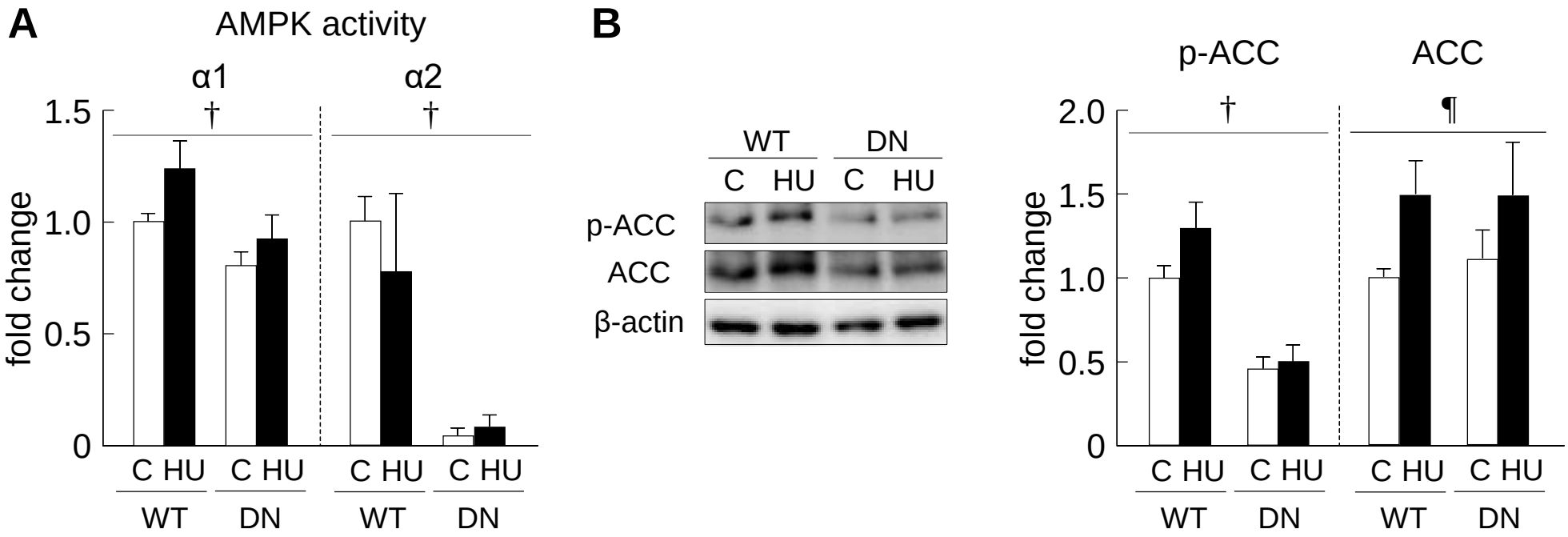
A
AMPK activity
α1
α2
†
†
1.5
1.0
0.5
0
fold change
C HU C HU C HU C HU
WT DN WT DN
B
WT DN
C HU C HU
p-ACC
ACC
β-actin
p-ACC
ACC
†
¶
2.0
1.5
1.0
0.5
0
fold change
C HU C HU C HU C HU
WT DN WT DN

Figure 1

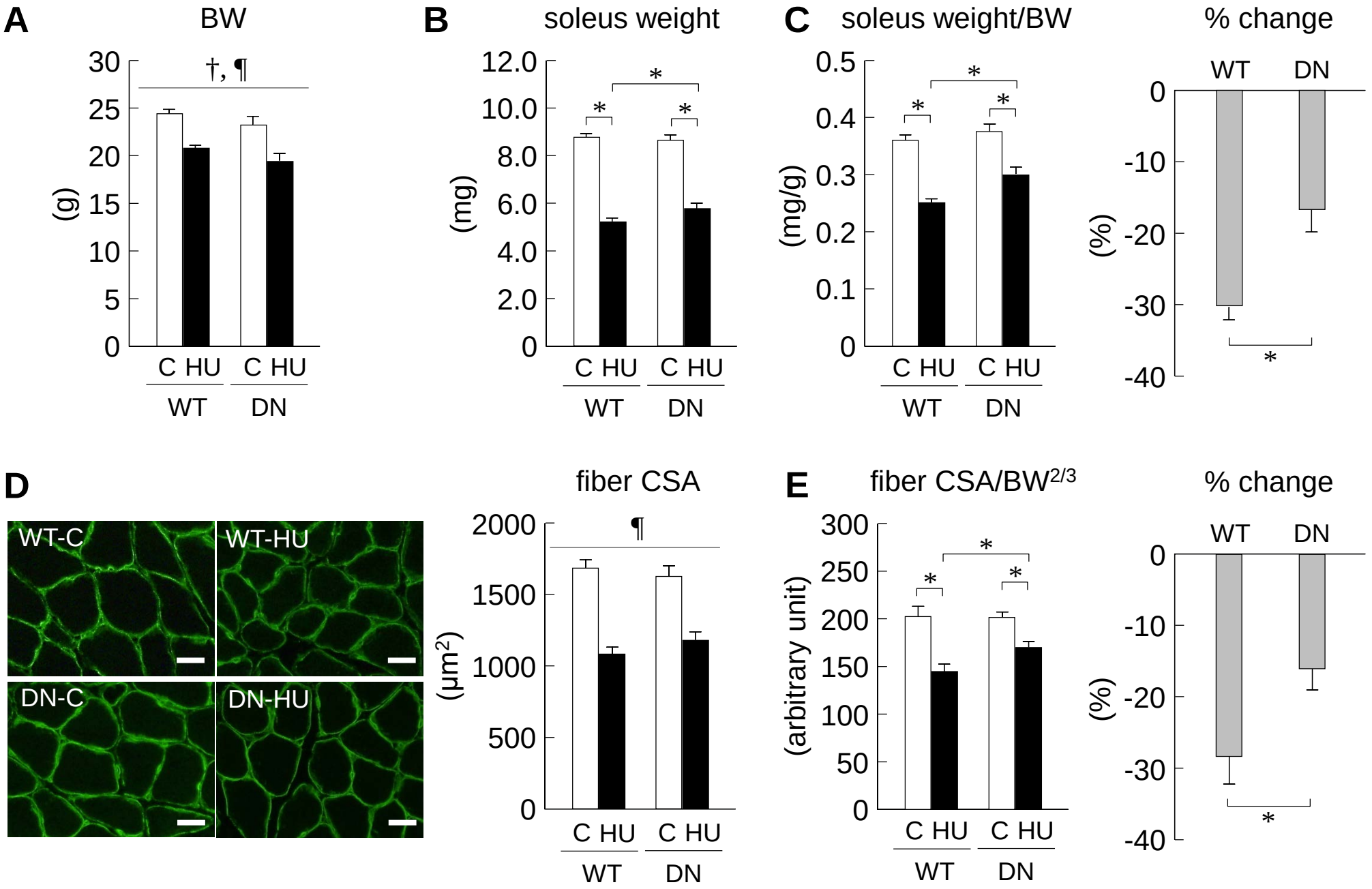
A
BW
(g)
†, ¶
C HU C HU
WT DN
B
soleus weight
(mg)
*
C HU C HU
WT DN
C
soleus weight/BW
(mg/g)
*
C HU C HU
WT DN
% change
WT DN
(%)
*
D
WT-C
WT-HU
DN-C
DN-HU
fiber CSA
(μm²)
¶
C HU C HU
WT DN
E
fiber CSA/BW^2/3
(arbitrary unit)
*
C HU C HU
WT DN
% change
WT DN
(%)
*

Figure 2

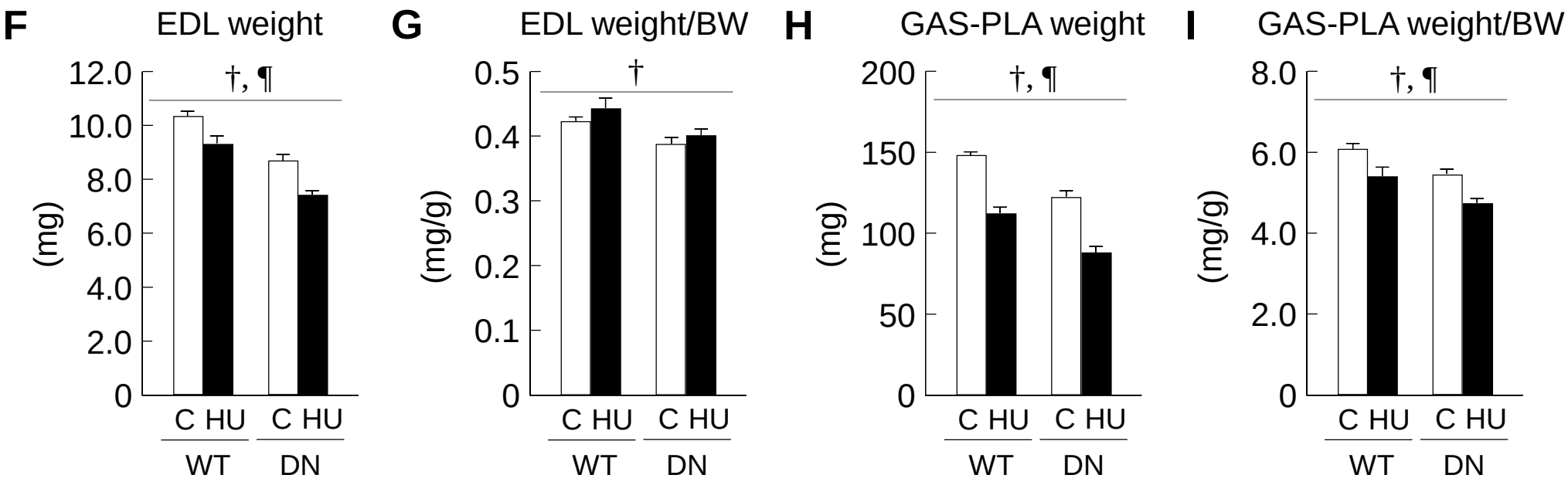
F
EDL weight
(mg)
12.0
10.0
8.0
6.0
4.0
2.0
0
†, ¶
C HU C HU
WT DN
G
EDL weight/BW
(mg/g)
0.5
0.4
0.3
0.2
0.1
0
†
C HU C HU
WT DN
H
GAS-PLA weight
(mg)
200
150
100
50
0
†, ¶
C HU C HU
WT DN
I
GAS-PLA weight/BW
(mg/g)
8.0
6.0
4.0
2.0
0
†, ¶
C HU C HU
WT DN

Figure 2

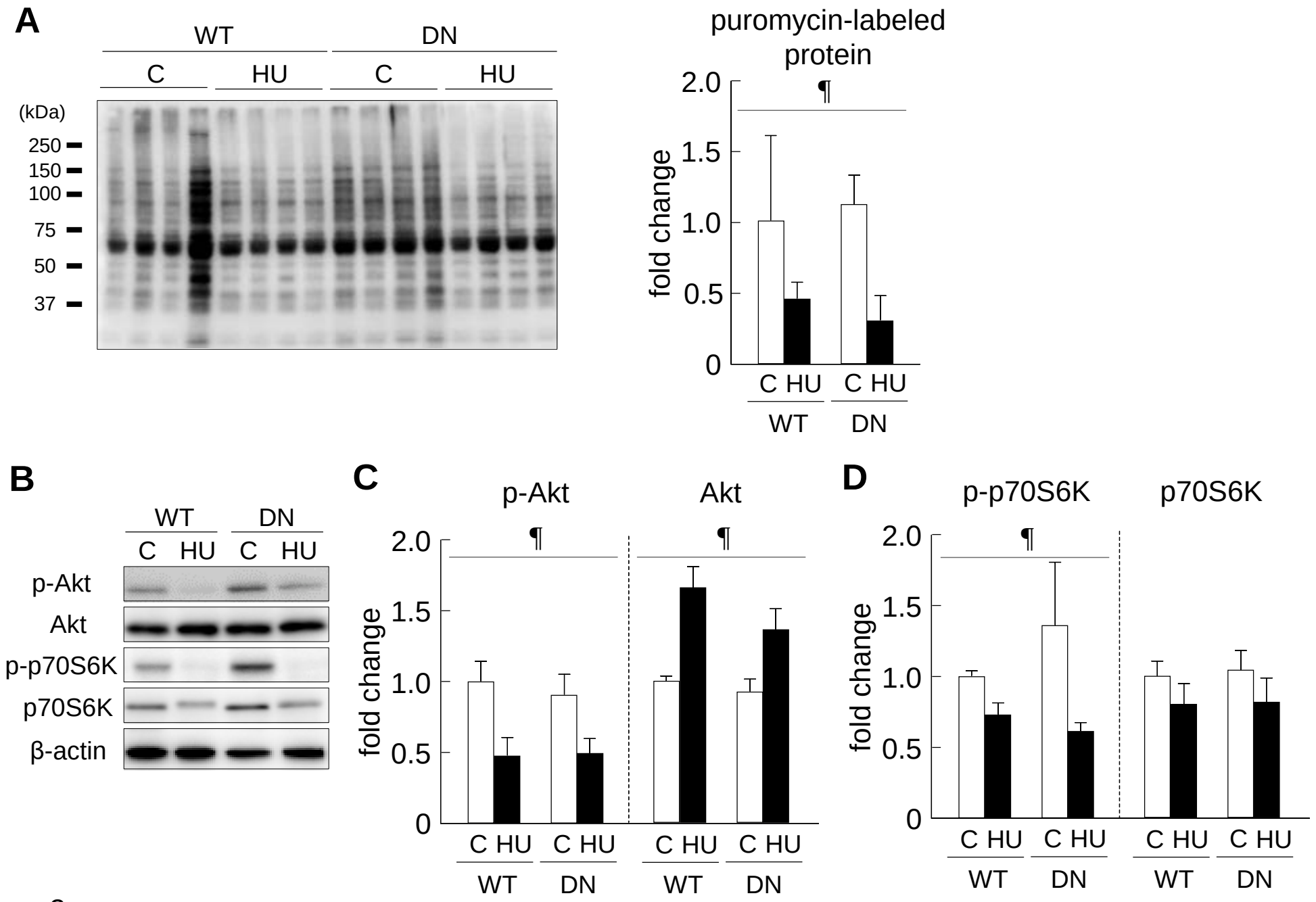
A
WT
DN
C
HU
C
HU
(kDa)
250
150
100
75
50
37
puromycin-labeled protein
¶
2.0
1.5
1.0
0.5
0
fold change
C HU C HU
WT DN
B
WT
DN
C HU C HU
p-Akt
Akt
p-p70S6K
p70S6K
β-actin
C
p-Akt
Akt
¶
¶
2.0
1.5
1.0
0.5
0
fold change
C HU C HU C HU C HU
WT DN WT DN
D
p-p70S6K
p70S6K
¶
2.0
1.5
1.0
0.5
0
fold change
C HU C HU C HU C HU
WT DN WT DN

Figure 3

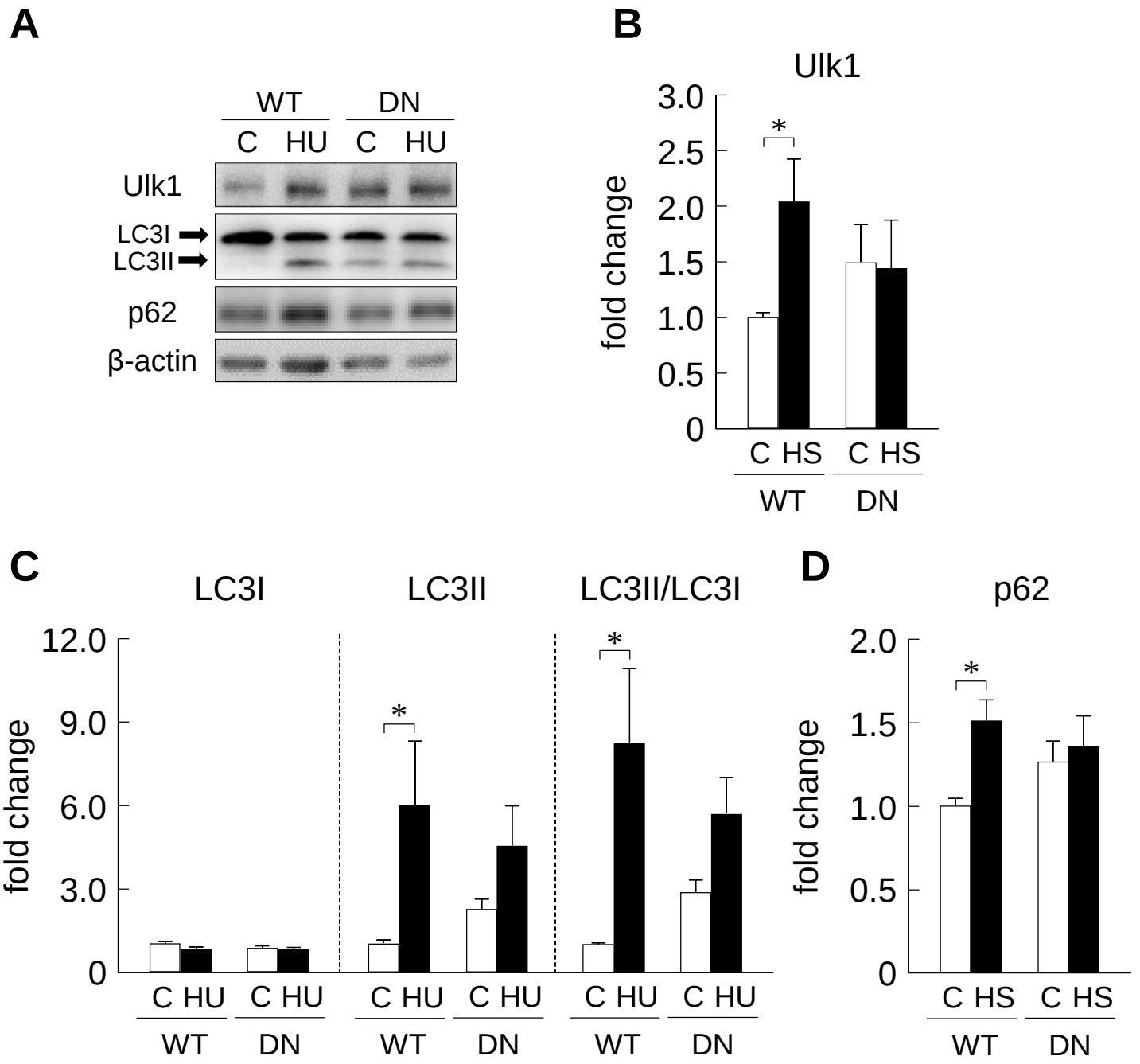
A
WT
DN
C
HU
C
HU
Ulk1
LC3I
LC3II
p62
β-actin
B
Ulk1
fold change
3.0
2.5
2.0
1.5
1.0
0.5
0
*
C HS C HS
WT DN
C
LC3I
LC3II
LC3II/LC3I
fold change
12.0
9.0
6.0
3.0
0
*
*
C HU C HU C HU C HU C HU C HU
WT DN WT DN WT DN
D
p62
fold change
2.0
1.5
1.0
0.5
0
*
C HS C HS
WT DN

Figure 4

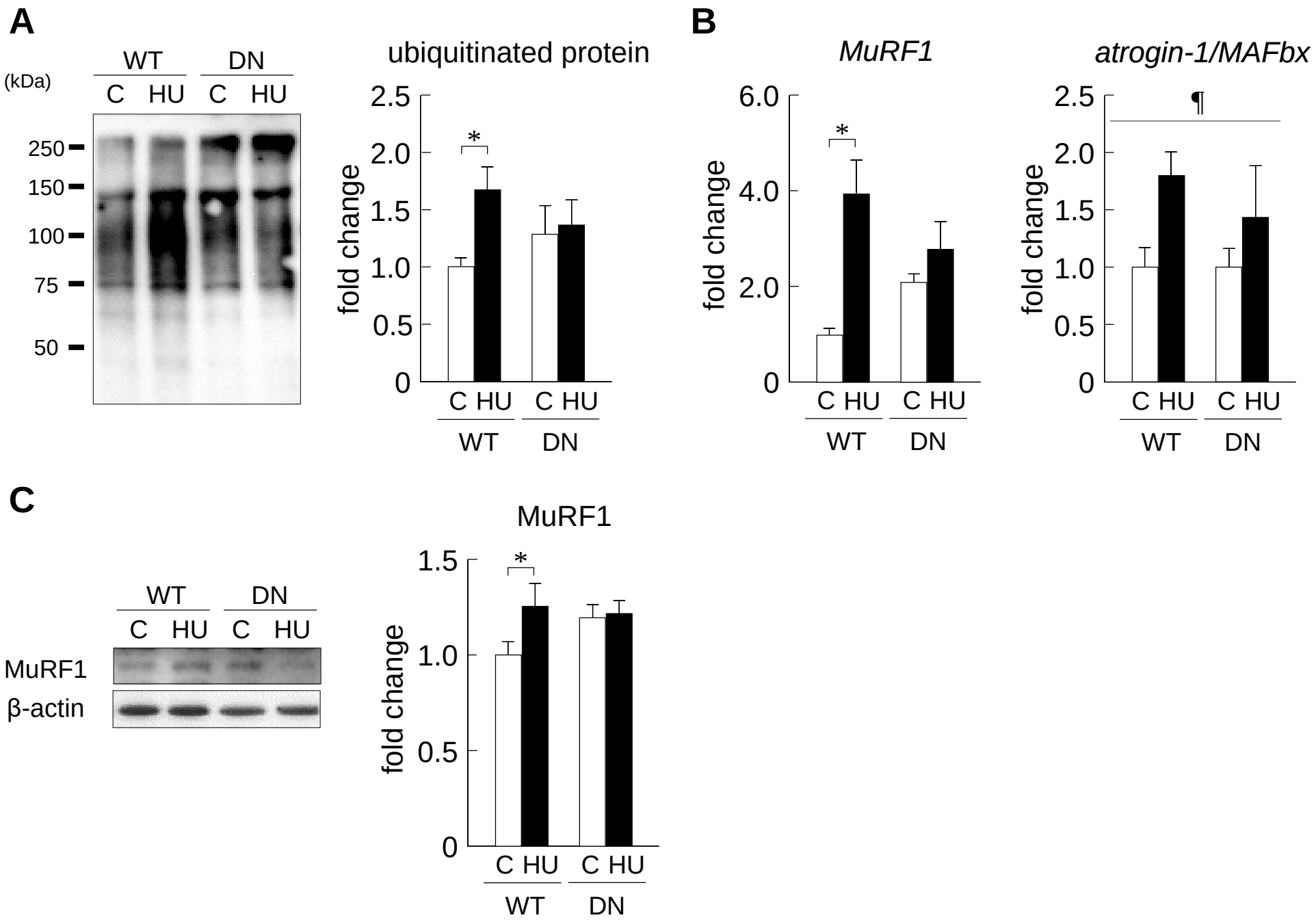
A
WT
DN
(kDa)
C HU C HU
250
150
100
75
50
ubiquitinated protein
fold change
2.5
2.0
1.5
1.0
0.5
0
*
C HU C HU
WT DN
B
MuRF1
6.0
4.0
2.0
0
*
atrogin-1/MAFbx
¶
C
WT
DN
C HU C HU
MuRF1
β-actin
MuRF1
1.5
1.0
0.5
0

Figure 5

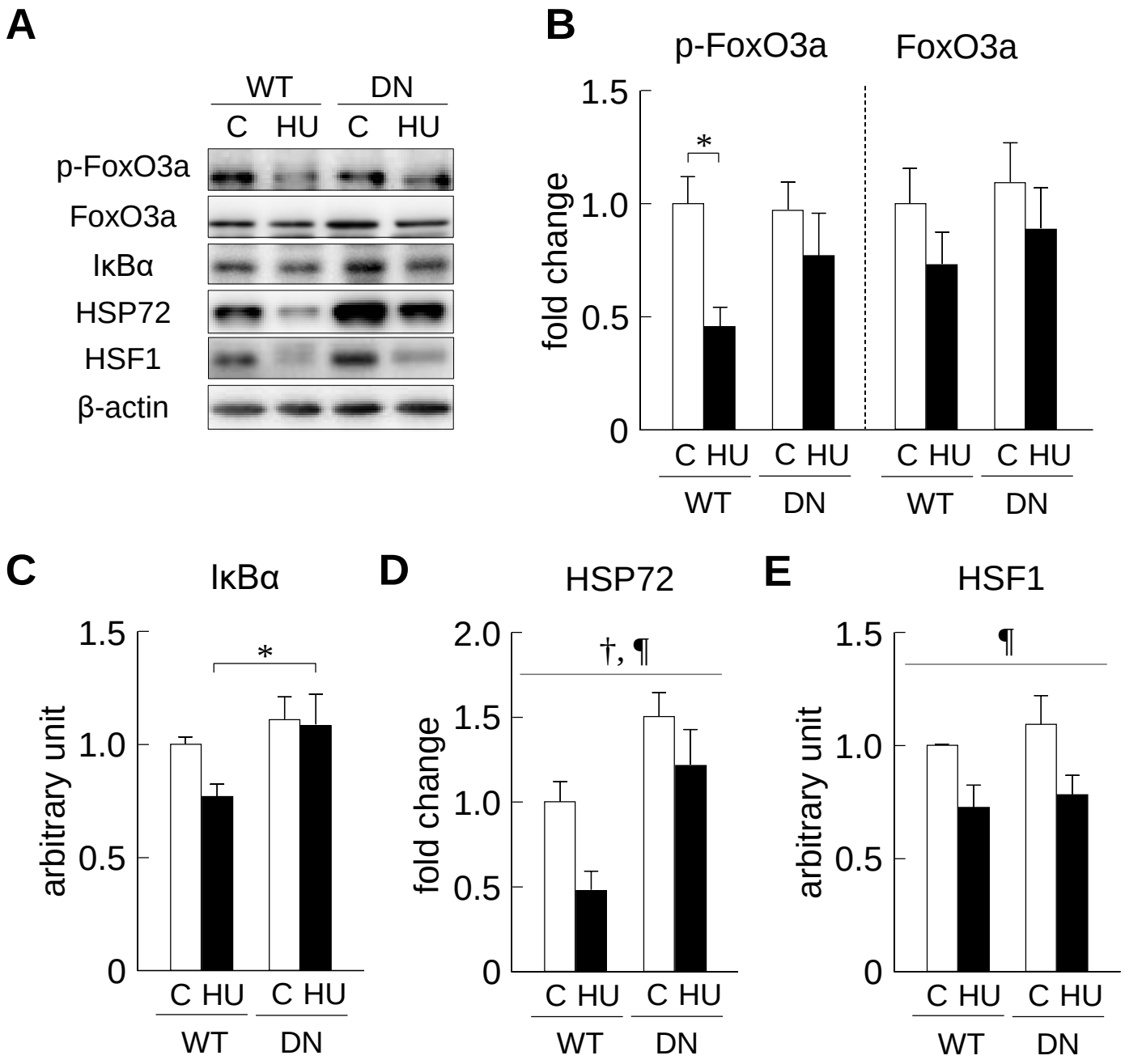
A
WT
DN
C
HU
C
HU
p-FoxO3a
FoxO3a
IκBα
HSP72
HSF1
β-actin
B
p-FoxO3a
FoxO3a
fold change
1.5
1.0
0.5
0
*
C HU C HU C HU C HU
WT DN WT DN
C
IκBα
arbitrary unit
1.5
1.0
0.5
0
*
C HU C HU
WT DN
D
HSP72
fold change
2.0
1.5
1.0
0.5
0
†, ¶
C HU C HU
WT DN
E
HSF1
arbitrary unit
1.5
1.0
0.5
0
¶
C HU C HU
WT DN

Figure 6

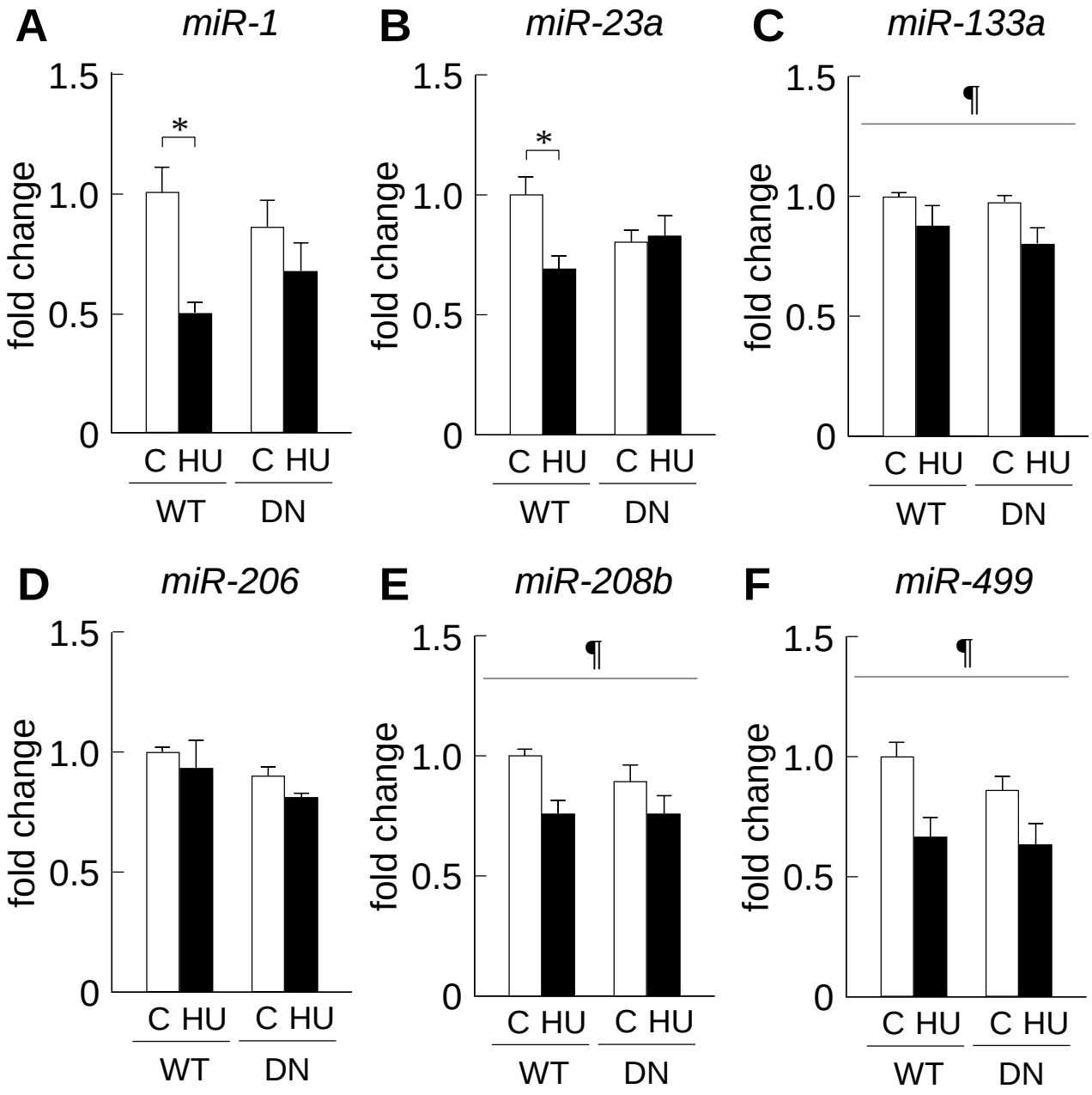
A
miR-1
B
miR-23a
C
miR-133a
D
miR-206
E
miR-208b
F
miR-499
fold change
1.5
1.0
0.5
0
*
¶
C HU C HU
WT DN

Figure 7